Contents lists available at ScienceDirect

Applied Energy

journal homepage: http://ees.elsevier.com

Tailoring of the pore structures of wood pyrolysis chars for potential use in energy storage applications

Przemyslaw Maziarka [a,*], Peter Sommersacher [b], Xia Wang [c], Norbert Kienzl [b], Stefan Retschitzegger [b], Wolter Prins [a], Niklas Hedin [c], Frederik Ronsse [a]

[a] Thermochemical Conversion of Biomass Research Group, Department of Green Chemistry and Technology, Faculty of Bioscience Engineering, Ghent University, Coupure Links 653, 9000 Gent, Belgium
[b] BEST – Bioenergy and Sustainable Technologies GmbH, Inffeldgasse 21b, 8010 Graz, Austria
[c] Department of Materials and Environmental Chemistry, Stockholm University, SE, 10691 Stockholm, Sweden

ARTICLE INFO

Keywords
Pyrochar
Temperature
Specific surface area
Tailoring
Supercapacitor electrode

ABSTRACT

Char obtained from biomass pyrolysis is an eco-friendly porous carbon, which has potential use as a material for electrodes in supercapacitors. For that application, a high microporous specific surface area (SSA) is desired, as it relates to the accessible surface for an applied electrolyte. Currently, the incomplete understanding of the relation between porosity development and production parameters hinders the production of tailor-made, bio-based pyrochars for use as electrodes. Additionally, there is a problem with the low reliability in assessing textual properties for bio-based pyrochars by gas adsorption. To address the aforementioned problems, beech wood cylinders of two different lengths, with and without pre-treatment with citric acid were pyrolysed at temperatures of 300–900 °C and analysed by gas adsorption. The pyrolyzed chars were characterised with adsorption with N_2 and CO_2 to assess the influence of production parameters on the textual properties. The new approach in processing the gas adsorption data used in this study demonstrated the required consistency in assessing the micro- and mesoporosity. The SSA of the chars rose monotonically in the investigated range of pyrolysis temperatures. The pre-treatment with citric acid led to an enhanced SSA, and the length of the cylinders correlated with a reduced SSA. With pyrolysis at 900 °C, the micro-SSAs of samples with 10 mm increased by on average 717 ± 32 m^2/g. The trends among the investigated parameters and the textual properties were rationalized and provide a sound basis for further studies of tailor-made bio-based pyrochars as electrode materials in supercapacitors.

1. Introduction

With an increase in social awareness, the pressure on the development of sustainable technologies has increased over recent years. Within this trend, annual growth in zero and low emission transportation with electric and hybrid vehicles is strongly visible [1,2]. One current research focus in electromobility is related to the optimisation of energy storage solutions in vehicles, which involves, for example, optimal coupling of energy-dense batteries with power-dense supercapacitors [1,3]. These components differ significantly when it comes to energy and power storage, involving physical and chemical mechanisms, as well as their lifespan [1]. In terms of power/energy handling, batteries have high specific energy storage capacity, but their specific power capacity is relatively low [4]. Supercapacitors have, on the other hand, relatively low energy storage capacity, but their specific power capacity is high [5]. New solutions for electric vehicles are based on coupled battery-supercapacitor systems, which allow for increasing their range, e.g. through energy recovery by means of supercapacitors during regenerative braking of the battery electric vehicle [1,3].

In supercapacitors, the electrode material presents the majority of the cost [6,7], which drives the research of new, less expensive and simultaneously environmentally friendly electrode materials. Porous carbon materials from bio-based origin like activated carbons and pyrochars have a low cost due to low feedstock prices (if sourced from, e.g. agroforestry residues) and desired properties (good electrical conductivity, high chemical and thermal stability, and due to an appropriate porous structure, good rectangular shape of the cyclic voltammetry curves and symmetrical galvanostatic charge-discharge profile) [8,9], which render them attractive as materials for electrodes [10,11]. Numerous application-related studies have proven that bio-based activated carbons [12–14] as well as pyrochars [15–17] show satisfactory results as electrode material for supercapacitors.

* Corresponding author.
E-mail address: Przemyslaw.Maziarka@UGent.be (P. Maziarka)

https://doi.org/10.1016/j.apenergy.2020.116431
Received 23 July 2020; Received in revised form 23 December 2020; Accepted 29 December 2020
Available online xxx

The performance of a material in a supercapacitor electrode is strongly related with the double-layer capacitance, hence it is related to the surface area accessible to an applied electrolyte [8,18]. However, in some studies, the accessible area is treated interchangeably with the specific surface area (SSA). This assumption has led to a different accuracy in prediction of the double-layer capacitance which is caused by the SSA assessment method itself [19,20]. It was found that SSAs obtained by using correlations from the BET (Brunauer–Emmett–Teller) method show poor prediction ability [21,22]. In contrast, another study has shown that the SSA derived from pores with a size range between 0.7 nm and 15 nm have a linear correlation with the double-layer capacitance [23]. However, the range of pore width yielding the relevant SSA for the double-layer capacitance is not constant as it depends on the size of ions in the electrolyte [24,25]. Moreover, even if there is a substantial and relevant SSA in the desired pore size region, a lack of interconnectedness between pores can lead to their clogging, and thus to the poor performance of the electrode as its accessible SSA is not completely used [26,27]. Overall, most studies point out that the material for the electrodes of supercapacitor should have a high and accessible SSA in the microporous region. Optimal properties can be achieved when a balance between the energy storage related pores (range between 0.4 and 1 nm) and interconnecting pores (range of 1 nm and 2 nm) is obtained [20]. Therefore, it is beneficial to be able to engineer the porous structure and pore size distribution (PSD) by tailoring the production parameters. Bio-based pyrochars have such an ability of tailoring, which opens up the possibility of engineering electrode materials from pyrochars. Besides of applications in supercapacitor electrodes, the tailoring can be beneficial for other materials that can be obtained from pyrochars such as activated carbons as their properties would be related to both the properties of the pyrochar and the activation process used [21,28].

In the current state-of-the-art, there are though limitations in the tailoring of the PSD of the pyrochar, and it cannot be performed with very high accuracy. General descriptions of changes in the carbonaceous structure along with process parameters have been already proposed [29–31], but detailed and consistent mechanisms for the development of porosity have only been discussed in few studies [31–36]. We ascribe this lack of knowledge to that the numerous studies on SSA of pyrochars have only relied on analyses of N_2 adsorption data with the BET method, which is a non-pore specific method. Hence, these studies contain a very limited amount of information about the specific porous structure and might be significantly biased when for carbons with a significant micropore volume as for pyrochars in general [37,38]. The problem with the BET method for a reliable SSA assessment of bio-based pyrochars has been shown by a cooperative analysis between eight laboratories [39] as well as by a broad data analysis [40]. Lately, a tendency towards a more detailed assessment of the pyrochar structure has been noticed [33,41,42]. Such studies consist of measurements of the adsorptive uptake and release of various probe gases (N_2, Ar, CO_2), and data analysis with pore-specific methods, which have been proven reliable through validation [43,44]. These approaches provide a PSD of a given material with an accurate SSA assessment in different pore size ranges (micro or meso) [45,46], allowing for a detailed description of pore structures, ultimately opening up the possible tailored production of bio-based pyrochars. Nevertheless, the number of available detailed studies is still low, and the knowledge gaps in relation to the mechanisms for the development of porosity in pyrochars are significant.

Some trends regarding how to tailor the porous structure of bio-based pyrochars are found in the literature. The temperature used in pyrolysis has a major effect on the porosity of the pyrochars, but the heating rate has only a minor influence [34]. The SSA of bio-based pyrochars usually increases up to a pyrolysis temperature of 700 °C with a sharp reduction above that temperature. Nevertheless, it is suspected that the nature of this observed SSA peak can be purely artificial [34]. When producing pyrochars on an industrial scale, which is typically done using larger feedstock particles, the increased particle radius is known to lower the heating rate. In contrast, the effect of changing the length of the particle on the porous structure has not been investigated yet. The latter question is quite relevant as on a larger scale, typically oblong feedstock particles are used (like pellets, logs, etc.). An increase in the length can lead to a longer residence time of pyrolysis volatiles within the structure. It is suspected that above 500 °C such longer residence times can lead to enhanced deposition of secondary char due to cracking of evolved volatiles [47], and in consequence causes a distortion in the PSD of the pyrochar. The mineral matter and its composition is also an adjustable feedstock property, and it affects the development of the pore structures of the pyrochars as well. A high concentration of mineral matter in the biomass feedstock can lead to the closing of pores through softening of mineral matter during the high-temperature conversion [48]. Additionally, the alkali and alkaline earth metals (AAEMs) within the feedstock can lead to a reduction in the SSA by a catalytic effect on devolatilisation [49,50]. To adjust the mineral matter content and to mitigate the aforementioned problems, acid leaching can be applied before pyrolysis. However, this leaching can also cause a degradation of the macromolecular components of the biomass [51] and thus influencing the pore development and complicating the tailoring of the PSD of the pyrochar.

This study has been conducted to investigate the possibility of detailed tailoring of bio-based pyrochars with a future application as electrode materials in supercapacitors. To reliably assess the influence of the temperature on the pore structure development, cylinders from beech wood were pyrolysed at five different temperatures ranging from 300 to 900 °C. Additionally, two lengths of cylinders were used, and citric acid leaching was applied in half of the samples. Accurate assessment of the micropores and mesopores was done by analyses of recorded CO_2 and N_2 adsorption data. The gas adsorption data were analysed using simple (non-pore specific) and more advanced (pore specific) methods to further assess deviations and biases. To support the observed trends, the elemental composition of the pyrochars were determined, and SEM and TEM studies of the morphologies were conducted. Within the study, the focus was also on proposing a consistent way of data processing which could accelerate future studies of tailored bio-based pyrochars in applications as electrode materials.

2. Methodology and materials

2.1. Wooden particles

In this study, beech wood cylinders of 8 mm in diameter and two different lengths (10 mm and 16 mm) were used, which resulted in samples with an aspect ratio close to 1 (1:1.25) and 2 (1:2) respectively. The length was selected in the same direction as the longitudinal direction of the wood fibres. Beech wood was selected due to its presumed low concentration of AAEMs [52–54]. Cylinders of both sizes were provided in bulk by Rundstäb (Meyer & Weigand GmbH, Nördlingen, Germany). The cylinders were machine-cut which guaranteed their high consistency in size and shape. The average deviation in diameter and length did not exceed 0.1 mm. Prior to pyrolysis, all samples were drilled in their geometrical centre with a drill bit of size Ø0.6 mm, and a drill-stand, to achieve a proper alignment of the drilled hole in each particle. Within the drilled hole, a thermocouple was installed in the centre of the wood cylinder.

2.2. Sample pre-treatment

The acid leaching procedure was based on the work of Rodríguez-Machín et al. [51]. The leaching pre-treatment was conducted in batches of 40 particles with the use of a 0.5 mol/dm^3 aqueous solution

of citric acid (prepared from 99% wt. citric acid, Sigma-Aldrich). Cylinders with a length of 10 mm and 16 mm were leached with 1 dm^3 and 2 dm^3 of leaching agent, respectively. That corresponds to approx. 0.005 g of pure citric acid per 1 cm^3 of dry beech wood. The cylinders were leached with continuous mixing of the citric acid solution for 8 h at 25 °C. After leaching, samples were neutralised by washing with demineralised water three times. Next, the samples were additionally soaked in fresh demineralised water for 8 h while mixing, which allowed removing the leftovers of the acid from the inner pores. After that, the samples were washed with fresh water for a last time. The samples not subjected to leaching pre-treatment were washed only once with demineralised water to remove any possible surface contamination. All samples were dried at 105 °C to a constant weight (for 24 h). In total, the preparation procedure resulted in four types of samples: non-leached and leached with length 10 mm (U1 and W1, respectively) and non-leached and leached with length 16 mm (U2 and W2, respectively).

2.3. Pyrolysis experiments

Each cylinder was pyrolysed individually in a Single Particle Reactor (BEST GmbH, Graz, Austria). The details about the construction of the reactor can be found in the publications of Sommersacher et al. [55,56] and its simplified scheme is presented in the work of Anca-Couce et al. [57]. Pyrolysis of a single sample type was performed at five temperatures: 300 °C, 400 °C, 500 °C, 700 °C and 900 °C, each in six repetitions. The flow of N_2 was set to 10 Ndm^3/min for all pyrolysis experiments. The pyrolysis temperatures were selected to contain three scenarios without secondary cracking of volatiles and three scenarios where secondary cracking will most likely occur. A temperature of 500 °C was selected as a threshold above which the secondary cracking of volatiles becomes significant [47]. Additionally, the lowest three temperatures were selected to indirectly investigate the influence of selective degradation of biomass constituents (hemicellulose, cellulose and lignin) [58]. The procedure of pyrolysis was based on the work of Anca-Couce et al. [57]. Initially, the reactor was heated up to the appropriate temperature (350 °C, 480 °C, 570 °C, 820 °C and 1050 °C respectively) prior to the introduction of a feedstock cylindrical particle. Then, the particle with mounted thermocouples (centre and surface), placed on a balance and covered by a cooling jacket, was inserted into the reaction zone of the reactor. The use of a cooling jacket prevented the sample from premature conversion, hence it allowed to adhere to a strictly controlled retention time. The temperature of the reactor was set higher than the desired pyrolysis temperature to compensate for the cooling effect of the sweep gas and thermal losses of the reactor. After the introduction of the particle into the reactor, the cooling jacket was removed, and the sample stayed in the reactor until its full conversion. For samples pyrolysed at 300 °C, the time of pyrolysis was set to 15 min, and for those pyrolysed at °C, 500 °C and 700 °C to 10 min, and for those pyrolysed at 900 °C to 5 min. For each temperature, the conversion time was sufficient to reach a stable temperature in the centre of the particle (within 10 s the variation was lower than 1% in relative terms). After the conversion, the cooling jacket was put back on the particle and the then the sample was flushed with N_2 to rapidly cool it down and prevent oxidation. When the sample reached ambient temperature, it was removed from the reactor. For all investigated samples, the heating rate at any point in the particle did not exceeded 50 °C/s. Therefore, particles were pyrolysed in the regime of intermediate/slow pyrolysis, typical for production of bio-based pyrochars. Exemplary temperature and heating rate profiles at the centre and surface of the non-leached beech wood cylinders with a length of 10 mm (U1) for every temperature of pyrolysis are presented in the Supplementary Information (Fig. S1-2).

2.4. Analytical measurements

2.4.1. Mineral matter and bio-composition

Inductively coupled plasma optical emission spectrometry (ICP-OES, Agilent Technologies 700 Series) was used to determine the composition of mineral matter in both types of used beech wood. The procedure of measurement was done according to Ovsyannikova et al. [59]. The major fractions of bio-components (cellulose, hemicellulose, lignin) in both types of used beech wood were determined using a modified Van Soest's method, accordingly to Reza et al. [60].

2.4.2. Homogenisation of pyrochar samples

From six repetitions, three samples with the highest outcome consistency (mass loss and centre temperature evolution) were selected for further analysis. Selected samples were ground in an agate mortar prior to analytical measurements. The grinding procedure was conducted to obtain appropriate homogenisation and to minimize the influence of the macro-structure on the measurements.

2.4.3. Elemental analysis

The samples were pre-dried overnight at 105 °C before elemental analysis. The mass fractions of carbon, hydrogen, nitrogen and sulphur were determined in triplicate on a dry basis (wt.%, db), using a Flash 2000 elemental analyser (Thermo Scientific). The oxygen mass fraction was calculated by difference.

2.4.4. Scanning and transmission electron microscopy

A scanning electron microscope (SEM, JEOL JSM-7000, Japan) was used to investigate the morphology of the samples pyrolysed at different temperatures. Prior to analysis, samples were placed on the SEM sample stud coated with a double-side tape. To further observe the detailed pore structure, transmission electron microscopy (TEM) experiments were performed on a field-emission electron microscope JEOL JEM-2100F, operating at 200 kV. Powdered samples were ultrasonically dispersed in ethanol for 15 s, one drop was transferred onto copper grids coated with holey carbon films and then dried before measurements.

2.4.5. Gas adsorption

Samples were degassed at 180 °C for 24 h before adsorption measurement. The low-temperature adsorption of N_2 was carried out at 77 K with a P/P_0 (N_2) range of 10^{-3} to 0.99. Adsorption of CO_2 was recorded at 273 K with a P/P_0 (CO_2) range of $5 \cdot 10^{-5}$ to 10^{-3}. The measurements were conducted on a Nova 4000e analyser (Quantachrome Instruments) equipped with an appropriate Dewar vessel for each gas adsorption measurement. In the case of repeated measurements, data from the first measurement were always used and not the average from consecutive measurements. This selection was performed to avoid a possible influence of consecutive measurements on the result (especially critical for N_2 adsorption analysis at 77 K).

2.4.6. Specific surface area and pore volume calculation

All computation of results has been performed using the NovaWin software from Quantachrome. The description of the theoretical foundations of the applied calculation methods is found elsewhere in the literature [43,61]. For processing data from measurements with N_2 only the adsorption isotherms were used [61]. The SSA and PSD were calculated from the N_2 adsorption isotherms using the non-pore specific, BET multipoint method and the pore specific, BJH (Barrett-Joyner-Halenda) method. The selection of the P/P_0 range for the BET multipoint calculation was performed in accordance with the guidelines [37,38]. Therefore for the BET method, the P/P_0 range from which the SSA was calculated and corresponding C-value is additionally provided. The BJH

model was calculated on the same P/P_0 range for every sample, and it covered pore sizes between 1 nm and 50 nm. From measurements with CO_2, both adsorption and desorption isotherms were used for further processing. The CO_2 sorption isotherms were processed with the non-pore specific, DR (Dubinin-Radushkevich) method, and as the pore specific method, the GCMC (Grand Canonical Monte Carlo) was applied. The GCMC method calculation was based on the whole P/P_0 range of CO_2 adsorption, and it corresponded to the PSD between 0.35 nm and 1.6 nm.

The DFT (Density Functional Theory) methods like NLDFT (Non-Local) or QSDFT (Quenched-Solid) were not applied to obtain the PSDs. The analytically based BJH method was selected with the knowledge of lower accuracy than methods based on numerical fitting [37]. However, the use of such a model is not restricted by access to specific software, so the processing procedure can be easily repeated. The only exception to this approach was the assessment of PSDs from CO_2 adsorption because the HK (Horvath–Kawazoe) method did not allow for obtaining the appropriate precision of the PSD.

2.4.7. Micropores and mesopores assessment form merged datasets

To assess the SSA and pore volume (V_{pore}) of micropores and mesopores, the PSDs from both gas adsorption measurements (N_2 and CO_2) were merged into one. The PSDs from both gas adsorption had an overlapping range in the area of micropores. The CO_2 adsorption is more accurate for micropore assessment [61], so for the overlapping region, the data from GCMC (CO_2) was used. The overall approach of the calculation procedure is presented in Fig. 1. The obtained (merged) dataset covered the pore size range from 0.35 nm to 50 nm. Next, the full range was divided into ranges corresponding to a certain type of pores. For micropores, this range was from 0.35 nm to 2 nm and for mesopores from 2 nm to 50 nm, accordingly to IUPAC's guidelines [37]. This procedure has already been applied in another study related to activated carbons from bio-based precursors, and it gave accurate and reliable results [48].

3. Results and discussion

3.1. Influence of leaching pre-treatment

The obtained bio-composition of the non-leached beech wood was in good agreement with other studies [62,63]. As presented in Table 1, the leaching pre-treatment with citric acid caused a noticeable reduction in the content of hemicellulose, and a corresponding increase in the content of cellulose. However, the concentration of lignin stayed relatively similar. Although the concentration of citric acid was only half of what was proposed in the study of Rodríguez-Machín et al. [51], the hemicellulose still underwent partial hydrolysis. These results indicate a very high sensitivity of hemicelluloses to acid treatments, even when weak organic acids are used. As in other investigations of beech wood [52–54], the initial concentration of AAEMs in beech wood was low. Nevertheless, leaching with citric acid reduced the concentration of AAEMs with 70 wt. %. Potassium, considered as most influential on the mechanism of pyrolysis devolatilisation [50], was removed almost completely during the leaching, and other elements (magnesium and calcium) were removed with an efficiency close to 50 wt. %.

3.2. Char yield and elemental composition

Characteristic trends of char yields and their elemental compositions [32,64] were observed for investigated samples as presented in Table 2. For all samples pyrolysed at 900 °C, the carbon content was the highest (close to 90 wt. %), and oxygen and hydrogen contents were the lowest (10 wt. % and 1 wt. %, respectively). However, for pyrolysis at 700 °C, the results were not substantially different. When a 6 mm longer wood particle was used, the char yield was enhanced, but the use of longer wood particles did not influence the elemental composition of the pyrochar. The leached beech wood cylinders (W) showed a higher concentration of carbon and a lower concentration of oxygen by 2 wt. % in comparison to their non-leached (U) counterparts. For pyrolysis at 400 °C, the primary differences between untreated and pre-treated beech wood-derived pyrochars were diminished. Samples processed above 400 °C did not show a significant difference in the elemental composition due to the pre-treatment. It is an indirect proof that the initial differences in the elemental composition of chars (up to 400 °C) were caused by the leaching-related changes in the bio-composition [58]. For pyrolysis at 900 °C, a difference in composition was observed between sample U2 and W2. For sample U2, the carbon content was higher and oxygen content lower by c.a. 1 wt. % in comparison to its leached counterpart. It is suspected that such an out-

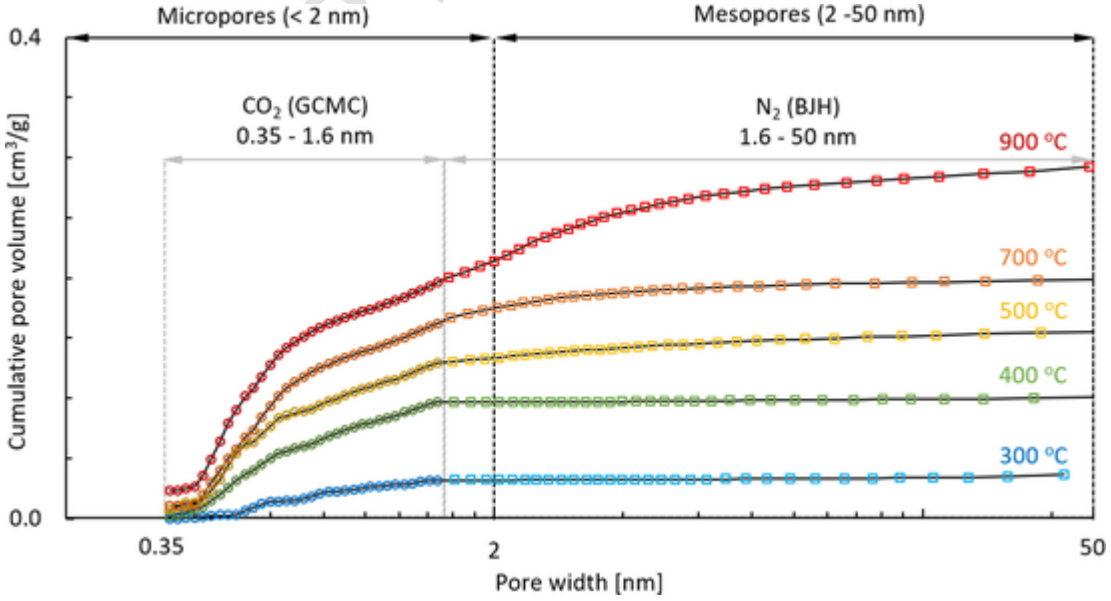

Fig. 1. Visualisation of the proposed assessment method for micropore and mesopore volume by merging and re-dividing the datasets from the different gas adsorption measurements.

Table 1
Bio-composition and mineral matter composition of non-leached (U) and leached (W) beech wood.

		Non-leached (U)	Leached (W)
Cellulose	[wt.%]	40.0 ± 0.3	41.7 ± 0.1
Hemicellulose	[wt.%]	34.1 ± 0.3	32.8 ± 0.2
Lignin	[wt.%]	25.9 ± 0.5	25.5 ± 0.1
Na	[mg/kg]	0*	0*
K	[mg/kg]	921	0*
Mg	[mg/kg]	315	162
Ca	[mg/kg]	891	447
AAEMs	[mg/kg]	2127	639

* - below detection limit, <10 mg/kg.
Ag, Al, B, Ba, Bi, Cd, Co, Cr, Cu, Fe, Ga, In, Li, Mn, Ni, Pb, Sr, Tl, Zn - below detection limit.

come could have been caused by a more substantial devolatilization of the U2 sample or deposition of secondary char on its pore surface, both related to the temperature-enhanced catalytic effect of AAEMs.

3.3. Gas adsorption isotherms and open hysteresis

The N_2 isotherms for pyrochars derived at 300 °C and 400 °C (provided in Fig. S3) had low volumes of both meso- and micropores. The isotherms of samples produced above 400 °C changed into IUPAC type I isotherm [37], which showed that microporous structures had developed in the pyrochars. The development of micropores was in agreement with analyses of the CO_2 adsorption isotherms, such isotherms are presented in Fig. S4. The uptake levels in the CO_2 isotherms showed that the volume of adsorbed CO_2 increased in the pyrochars prepared at the temperature above 400 °C. Analyses of both the N_2 and CO_2 isotherms are consistent with that the degradation of bio-components (especially cellulose and lignin) as expected led to significant changes in the wood structure and to the creation of microporosity, when the pyrolysis temperature was high enough.

For almost all samples, a strong discrepancy between the N_2 adsorption and desorption curves were observed, which may be caused by pore blocking phenomena [43]. Therefore, despite that an increase in the mesoporosity can be observed on the N_2 adsorption isotherms, no accurate information regarding the shape of the mesopores can be provided. The strong deviation between sorption curves, leading to their lack of meeting at the endpoint is called "open hysteresis", and it has been already observed in the literature especially for N_2 isotherms of bio-based pyrochars. However, the causes of its origin are still unclear. Several measurements of bio-based pyrochars with different gas adsorption methods (CO_2, Ar and benzene) as well as with ^{13}C NMR and FTIR spectroscopy suggest that the hysteresis can be related to irreversible pore swelling during adsorption [65]. It is suspected that in favourable conditions, the adsorbate (N_2) penetrating into the pores can cause deformation of their shape and in consequence lead to expansion of the pore volume during measurement. Other studies confirm that micro-structures of carbonaceous materials can undergo deformation, especially during low-temperature N_2 sorption [66,67]. It was also observed that with a higher temperature of the adsorption measurement, the deformation occurs less severely, which can be related to the lower strength of the interaction between the adsorbate and adsorbent as well as more dynamic diffusion of the adsorbate into pores [66,67]. In this study, the "open hysteresis" phenomenon did not occur very strongly in the CO_2 adsorption, as opposed to N_2 adsorption where is was strongly noticeable. Therefore, it is suspected that results from CO_2 adsorption are less likely to be biased due to structural deformation during adsorption.

Table 2
Yields and elemental composition of beech wood chars (P-T – pre-treatment type: U – non-leached, W – leached; AR – aspect ratio: 1 – Ø8 mm × 10 mm, 2 – Ø8 mm × 16 mm).

P-T	AR	Temp.	Yield	C	H
[–]	[–]	[°C]	[wt.%]	[wt.%]	[wt.%]
U	–	Raw	–	45.3 ± 0.2	6.0 ± 0.1
	1	300	59.5 ± 2.8	57.3 ± 0.5	5.5 ± 0.1
		400	25.8 ± 1.0	74.3 ± 0.1	3.7 ± 0.1
		500	20.0 ± 1.7	79.1 ± 0.1	3.2 ± 0.1
		700	13.2 ± 1.0	87.3 ± 0.3	2.0 ± 0.0
		900	10.5 ± 0.5	88.7 ± 0.4	1.2 ± 0.0
	2	300	63.6 ± 2.6	57.1 ± 0.1	5.5 ± 0.0
		400	25.6 ± 0.5	74.7 ± 0.3	3.8 ± 0.0
		500	20.8 ± 0.6	79.1 ± 0.2	3.2 ± 0.0
		700	14.0 ± 1.4	87.5 ± 0.5	2.1 ± 0.1
		900	11.5 ± 0.9	90.4 ± 0.2	1.0 ± 0.0
W	–	Raw	–	47.1 ± 0.1	6.1 ± 0.1
	1	300	59.9 ± 2.3	58.6 ± 0.0	5.2 ± 0.1
		400	24.5 ± 0.3	74.0 ± 0.3	3.6 ± 0.1
		500	20.1 ± 0.6	78.1 ± 0.0	3.0 ± 0.0
		700	10.5 ± 0.5	87.6 ± 0.1	2.2 ± 0.1
		900	8.7 ± 0.8	89.7 ± 0.1	1.1 ± 0.1
	2	300	64.8 ± 3.5	58.3 ± 0.2	5.5 ± 0.1
		400	25.7 ± 0.6	74.3 ± 0.3	3.7 ± 0.0
		500	20.5 ± 0.7	78.4 ± 0.2	3.2 ± 0.0
		700	12.4 ± 2.5	87.8 ± 0.1	2.3 ± 0.0
		900	11.3 ± 1.3	89.1 ± 0.5	1.1 ± 0.1

All data presented on a dry basis.

3.4. Differences in results from N_2 and CO_2

In Table 3, SSA values calculated using the BET method along with the P/P_0 range and the C parameter are shown. According to Rouquerol's restrictions for the BET method [38] for samples which show a high microporosity upon N_2 adsorption, the P/P_0 range has to be shifted to lower values to obtain a positive value of the C parameter. The latter value describes the energy of monolayer adsorption, so a negative value is not physically consistent [37]. The Rouquerol plots presented in Fig. S5 have been made to identify the appropriate range of P/P_0 values for each sample. The Rouquerol's plot for leached samples with 10 mm length (U1) and with an indication of P/P_0 ranges that are allowed to be used in the BET method is presented in Fig. 2. The typical range of P/P_0 (0.1–0.3) for the calculation of the SSA with the BET method could be applied only for samples produced at 300 °C,

Table 3
SSA and V_{pore} of beech wood pyrochars obtained from the N_2 and CO_2 adsorption and using different calculation methods (P-T – pre-treatment type: U – non-leached, W – leached; AR – aspect ratio: 1 – Ø8 mm × 10 mm, 2 – Ø8 mm × 16 mm).

P-T	AR	Temp.	N_2 adsorption					CO_2 adsorption			
			BET			BJH		DR		GCMC	
			P/P_0 (N_2)	C	SSA	SSA	V_{pore}	SSA	V_{pore}	SSA	V_{pore}
[–]	[–]	[°C]	[–]	[–]	[m^2/g]	[m^2/g]	[cm^3/g]	[m^2/g]	[cm^3/g]	[m^2/g]	[cm^3/g]
U	–	Raw	–	–	–	–	–	101	0.038	72	0.028
	1	300	0.10–0.30	22	1	2	0.005	203	0.076	138	0.046
		400	0.10–0.30	24	2	5	0.006	337	0.126	302	0.092
		500	0.02–0.06	746	60	44	0.028	455	0.171	444	0.130
		700	0.02–0.09	675	372	511	0.185	560	0.210	560	0.153
		900	0.10–0.30	14	74	188	0.114	785	0.295	783	0.201
	2	300	0.10–0.30	13	1	2	0.006	128	0.048	92	0.032
		400	0.10–0.30	107	1	1	0.004	331	0.117	290	0.088
		500	0.02–0.09	1764	20	15	0.015	406	0.152	399	0.116
		700	0.02–0.11	913	318	434	0.162	466	0.175	483	0.131
		900	0.10–0.30	23	52	133	0.072	635	0.239	639	0.163
W	–	Raw	–	–	–	–	–	87	0.033	67	0.026
	1	300	0.10–0.30	17	1	2	0.005	119	0.045	93	0.032
		400	0.10–0.30	61	1	2	0.004	339	0.127	313	0.097
		500	0.02–0.06	724	77	72	0.041	465	0.175	446	0.130
		700	0.01–0.03	1331	429	149	0.067	587	0.220	557	0.162
		900	0.10–0.30	13	95	208	0.122	776	0.291	722	0.196
	2	300	0.10–0.30	9	2	3	0.029	132	0.049	86	0.007
		400	0.10–0.30	18	2	3	0.091	310	0.117	295	0.005
		500	0.09–0.20	298	35	54	0.116	416	0.156	400	0.034
		700	0.01–0.03	870	513	218	0.158	539	0.202	534	0.091
		900	0.10–0.30	20	107	226	0.170	656	0.246	643	0.127

400 °C and 900 °C. For all samples produced at 500 °C and 700 °C, the P/P_0 range had to be shifted into a lower range, typical for activated carbons, which led to a higher C-value related to the formation of a gas monolayer in the microporous region. However, it needs to be highlighted that the shift of the P/P_0 range into the microporous region can artificially change the value of the SSA obtained by the BET method, even within the range allowed by Rouquerol's restrictions.

The comparison of SSA values obtained with N_2 adsorption and calculated with the BET and BJH methods showed a lack of agreement (Table 3). The SSA from the BJH method was calculated from a PSD which was based on a defined and constant P/P_0 range for every sample. On the opposite, the P/P_0 range applied in the calculation of SSA by the BET method was not consistent for every sample due to Rouquerol's restrictions. As can be noticed for samples produced at 500 °C and 700 °C, the deviation between both methods is the highest. Therefore, it is suspected that these differences can be caused by the P/P_0 range adjustment. Due to calculation consistency, the results obtained using the BJH method should be more reliable or at least burdened with a constant error in comparison to the BET method. However, the results from both the BET and BJH methods can still be biased in the microporous region due to structure swelling during the low-temperature N_2 adsorption.

Values for the SSA and pore volumes obtained from the CO_2 adsorption with the DR and GCMC method are also presented in Table 3. The difference in the SSA obtained with both methods was not substantial for pyrochars prepared above 300 °C. However, the DR method gave systematically higher values than the GCMC method for the pore volume (V_{pore}) in the whole investigated range. With the non-pore specific, DR method V_{pore} was assessed within the applied P/P_0 range, and

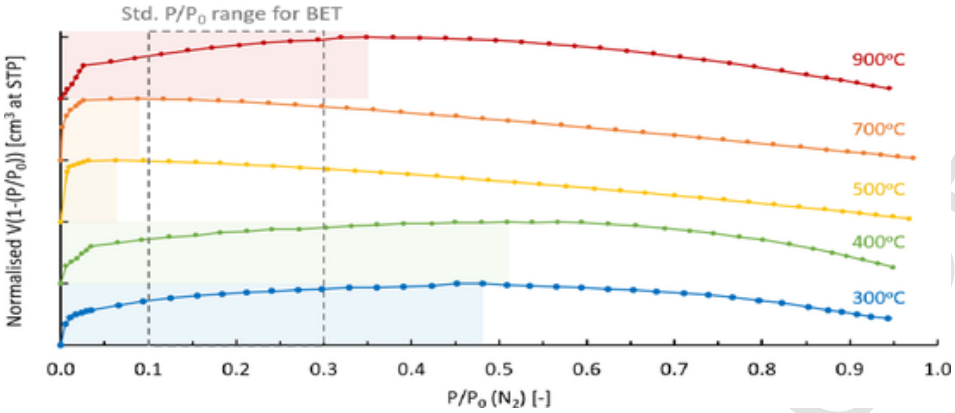

Fig. 2. Normalised Rouquerol's plots for U1 samples (coloured rectangle for each temperature – P/P_0 range that is allowed for BET method, grey lines – standard P/P_0 range).

then through the averaged pore width equation, the SSA was calculated. Using the pore selective GCMC method, the PSD was fitted to the CO_2 isotherm and then by summation the values of the SSA and V_{pore} were derived. As such, pore specific methods led to higher accuracy in the determination of SSA than the nonspecific methods. From the obtained results, it is suspected that the DR method compensated the larger pores (larger volumes, smaller SSA) with smaller pores (smaller volume, higher SSA). Then, due to the averaging, the values of the SSA from both methods were comparable despite of the significant difference in the obtained values for V_{pore}.

For each temperature series, the SSA and V_{pore} derived from N_2 adsorption data increased monotonically for with the pyrolysis temperature up to 700 °C. For pyrochars prepared at a temperature of 900 °C, a characteristic drop in the porosity volumes were observed for all types of samples (Table 3). In contrast, for results based on analyses of the CO_2 adsorption data, the SSA and V_{pore} increased monotonically with the pyrolysis temperature. Other studies of bio-based carbonaceous structures have indicated similar and consistent changes between pyrolysis temperatures of 500 °C and 900 °C [29,36]. Moreover, the peak in the temperature-dependent SSA and V_{pore} for pyrochars prepared at a temperature of 700 °C observed in the analyses of the N_2 adsorption data has also earlier been suspected to be artificial [34] and caused by micropore distortion (e.g. swelling) [65,66]. Therefore, the different trends with respect to the temperature-dependent porosities of pyrochars indicate that the N_2 analysis is burdened with systematic errors. The SSA and V_{pore} obtained by N_2 and CO_2 adsorption analyses are related to different ranges of the pore widths and temperature of experimentation, so it should be noted that a direct comparison of the adsorptive-dependent SSA and V_{pore} will lead to biased conclusions for materials such as pyrochars.

3.5. Systematic error in gas adsorption

To further investigate the systematic error of SSA methods and to assess differences between measurement techniques, consecutive measurements with N_2 (BJH) and CO_2 (GCMC) have been conducted for specific pyrochar samples. A sample prepared from leached wood, with a length of 16 mm (W2) and pyrolysed at a temperature of 700 °C was selected due to a suspected strong pore distortion during N_2 adsorption. The results of the SSA and V_{pore} derived from a specific pore width range is presented in Table 4. The deviation in pore volume between consecutive N_2 adsorption measurements was substantial in the micropore region. For pores with widths lower than 1 nm the deviation was ± 0.041 cm^3/g, and for pores in the range between 1 nm and 1.6 nm it was ± 0.028 cm^3/g. On the contrary for CO_2 adsorption, no large deviation was observed for pores with widths lower than 1 nm nor for pores in the range between 1 nm and 1.6 nm (± 0.008 cm^3/g and ± 0.000 cm^3/g, respectively). The measurement with N_2 adsorption to assess pores in the range from 1.6 nm to 2 nm and for the mesopores (from 2 nm to 50 nm), was not burdened with significant deviation and showed more than a satisfactory consistency.

Table 4
SSA and V_{pore} from consecutive gas adsorption measurements with N_2 and CO_2 of the leached sample with length 16 mm (W2) produced at 700 °C.
Expand

		Pore width range [nm]	Measurement		Standard deviation
			1st	2nd	
N_2 (BJH)	SSA [m^2/g]	< 1	383	586	± 144
		1–1.6	163	305	± 101
		1.6–2	23	26	± 2
		2–50	32	32	± 0
		Total	601	950	± 247
	V_{pore} [cm^3/g]	< 1	0.084	0.142	± 0.041
		1–1.6	0.049	0.089	± 0.028
		1.6–2	0.011	0.012	± 0.001
		2–50	0.030	0.030	± 0.000
		Total	0.173	0.272	± 0.070
CO_2 (GCMC)	SSA [m^2/g]	< 1	469	498	± 20
		1–1.6	36	36	± 0
		Total	505	534	± 21
	V_{pore} [cm^3/g]	< 1	0.124	0.135	± 0.008
		1–1.6	0.022	0.022	± 0.000
		Total	0.146	0.158	± 0.008

The overlapping region of the pore width from 1 nm to 1.6 nm analysed by using both N_2 and CO_2 adsorption data was compared to assess differences between both analyses techniques. For the selected range, the V_{pore} from derived from N_2 adsorption analysis was significantly higher than the one derived from CO_2 adsorption analysis. Volumes from N_2 measurement should be lower than the ones obtained from CO_2, considering that the low-temperature N_2 has a problem diffusing into smaller micropores as opposed to CO_2 [43]. It is suspected that N_2 adsorption could inflate the results of the microporous region due to deformation of the pore structure during measurement. Overall, for the overlapping region, the CO_2 measurement presents a more reliable outcome. For pores larger than 1.6 nm, the measurement with N_2

is consistent and does not indicate a significant burden of error, while in the standard setup for CO_2 adsorption analysis at 273 K, larger pores cannot be assessed. Therefore, during the merging of the PSDs obtained from analyses of N_2 (BJH) and CO_2 (GCMC) adsorption, data from CO_2 adsorption was used for the overlapping pore width range. However, it was noted that in the upper range towards 1.6 nm, the pressures of CO_2 accessible might have been somewhat too small.

To assess the influence of parameters used in the preparation of the pyrochars on the SSA and V_{pore}, a consistent method to process the data from both gas adsorption measurements (N_2 and CO_2) was applied. Since the applicability of the analyses depends on the number of pores with a certain size range, non-pore specific methods were not used because they do not provide a PSD. The proposed method is based on a pore specific calculation method, and used PSD up to 1.6 nm from CO_2 adsorption and above that pore width from N_2 adsorption. As can be noticed in Table 4, the selected approach provides a very low systematic error (e.g. 5% relative difference between consecutive measurements for sample W2 on SSA basis), out of which most was caused in the small micropore region (< 1 nm). Therefore, the proposed procedure for deriving PSD can be considered as a reliable and accurate assessment of micro- and mesopores in pyrochars. Additionally, the merged dataset allows for a quick derivation of the SSA with pores larger than the diameter of ions in the electrolytes allowing the applicability of the pyrochars as electrode materials in supercapacitors to be assessed qualitatively [18].

Table 5
SSA and V_{pore} of beech wood pyrochars obtained with proposed calculation method (P-T – pre-treatment type: U – non-leached, W – leached; AR – aspect ratio: 1 – Ø8 mm × 10 mm, 2 – Ø8 mm × 16 mm).
Expand

P-T	AR	Temp.	Micropores		Mesopores	
			Range: 0.35–2 nm		Range: 2–50 nm	
			SSA	V_{pore}	SSA	V_{pore}
[–]	[–]	[°C]	[m^2/g]	[cm^3/g]	[m^2/g]	[cm^3/g]
U	–	Raw	72	0.028	0	0.000
	1	300	138	0.047	1	0.005
		400	303	0.092	3	0.006
		500	450	0.133	11	0.015
		700	630	0.183	53	0.047
		900	812	0.214	66	0.076
	2	300	92	0.032	2	0.006
		400	290	0.088	1	0.004
		500	401	0.117	7	0.010
		700	545	0.158	51	0.046
		900	661	0.172	37	0.043
W	–	Raw	67	0.026	0	0.000
	1	300	93	0.032	1	0.005
		400	313	0.097	2	0.004
		500	456	0.134	17	0.021
		700	587	0.176	23	0.025
		900	761	0.214	77	0.079
	2	300	86	0.029	3	0.007
		400	295	0.091	2	0.005
		500	407	0.119	18	0.023
		700	574	0.175	32	0.032
		900	687	0.190	75	0.078

3.6. Influence of process parameters

The summary of the structural parameters from the merged PSDs for every sample is shown in Table 5. Values of microporous and mesoporous SSA and V_{pore} for each temperature series show a similar trend with an increase in temperature, and more importantly, parameters do not display a high random variation. Additionally, for all temperature series the pyrochars had a monotonic rise in the porosity with respect to the pyrolysis temperature and did not display a peak at 700 °C, which is in agreement with the studies on structural changes in bio-based carbonaceous materials with temperature, [29] and the collapse of pores in bio-based materials [36].

For all samples, the SSA in the microporous region was significantly higher than in the mesoporous region, as can be seen in Fig. 3. Despite differences in length and pre-treatment, the pyrochars showed strong similarity in the development of the micropores. When prepared at temperatures < 300 °C, the increase in SSA was negligible, and above that temperature, significant microporosity was noticed for the pyrochars. The difference in the microporous SSA between pyrochars prepared from wood cylinders of different length became noticeable for pyrolysis temperatures of 500–900 °C. The differences were consistent with that secondary char formation (char from thermal cracking of high molecular compounds), relevant at temperatures above 500 °C [47] was enhanced by an increased length of the wood cylinder. Vapours that evolved during the wood pyrolysis, due to a pressure difference move through the outer, highly-heated char layer. Considering that wood has a higher gas permeability in the longitudinal direction compared to the radial direction, the escape path of the volatiles is lon-

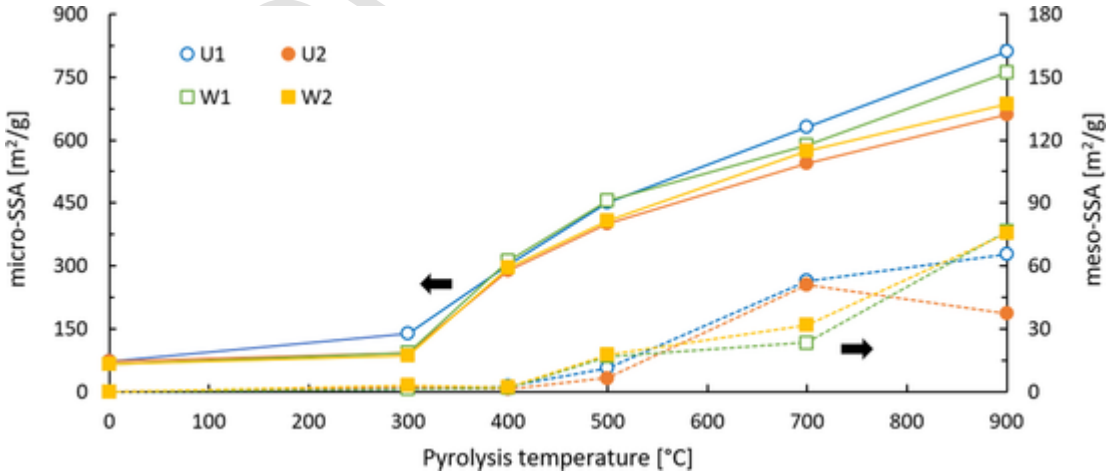

Fig. 3. Changes in the mesoporous and microporous SSA with pyrolysis temperature (left axis: microporous SSA – solid line, right axis: mesoporous SSA – dashed line; U – non-leached, W – leached; 1 – Ø8 mm × 10 mm, 2 – Ø8 mm × 16 mm).

gitudinally oriented. Therefore, with an increase in the particle length, the escape path of volatiles through the high-temperature zone became longer, hence, the residence time. In consequence, this appears to enhance the secondary char formation and reduction of the SSA. Overall, the increase in pyrolysis temperature from 300 °C to 900 °C led to an increase in the microporous SSA for the 10 mm particles by 671 ± 4 m^2/g and for the 16 mm particles by 585 ± 23 m^2/g. However, the influence of the leaching pre-treatment of the wood before pyrolysis had a minor and inconclusive effect on the microporosity of the pyrochars.

The mesoporous SSA development in the pyrochars had a less consistent trend with pyrolysis temperature than for the development of the microporous SSA. The mesoporous SSA of the pyrochars was more strongly dependent on the acid leaching pre-treatment than on differences in the particle length of the wood cylinders (Fig. 3). Up to pyrolysis temperatures of 400 °C, the mesoporosity had been barely developed in the pyrochars, and the differences in the pre-treatment were within the error margin of the measurements. Differences in the mesoporous SSA between pyrochars obtained from pre-treated and untreated wood became visible when prepared at temperatures from 500 °C and higher, as can be seen from the temperature-dependent mesoporous SSA of the pyrochars in Fig. 3. Considering that leaching led to a significant reduction of the catalytically active AAEMs, their reduced concentrations can be linked to a reduced mesoporous SSA. The most noticeable difference was obtained for the pyrochars prepared at 700 °C, where the non-leached samples presented almost a doubled mesoporous SSA in comparison to the leached samples. However, at the highest investigated temperature, similar values of the SSA indicates that the final mesoporosity was not affected strongly by the AAEMs, although the U2 sample had another trend. Similar conclusions have been presented in a study related to structural changes of carbonaceous materials [29], however, such phenomena are only related to low ash biomass since the mineral matter has the ability to catalytically influence the organisation of the carbonaceous structure [30].

Similar to the elemental composition (Table 2), the results of gas adsorption analyses for the non-leached sample (16 mm length) produced at 900 °C appeared to deviate from the observed trends in all other samples. For this sample (U2), it was suspected that the combined effect of temperature, length and AAEMs led to substantial enhancement of secondary cracking, which in consequence seemed to have altered the micro and mesoporosity as well as the carbon content. The temperature trends for the reduction of its mesoporous SSA was defined (see Fig. 3). The differences in the carbon content between the non-leached wood cylinders of 10 mm and 16 mm length, may suggest more carbon deposition on the internal surface for the longer pyrolysed cylinders. This deposition could speculatively have led to changes in the surface roughness and/or filling of pores and in consequence to an increase of the microporosity at the expense of mesoporosity. Due to a lack of conclusive results, the occurrence of this mechanism needs to be further investigated and validated.

3.7. Changes in the morphology of the materials

Assessment of the morphology of the pyrochars was conducted with SEM and TEM to validate the results from the gas adsorption analysis. Features in the SEM in Fig. 4 indicate that the structure of pyrochars prepared from non-leached (U) and leached (W) wood cylinders changed in a similar manner with an increased pyrolysis temperature. For pyrolysis at 300 °C, the char structures resembled the initial wood structure, which was related to incomplete conversion of cellulose and lignin. Increasing the temperature up to 500 °C led to a noticeable thinning of the cell wall structures in the pyrochars, caused by a severe degradation of the bio-components therein [58]. When pyrolysed at temperatures above 500 °C, further cell wall thinning occurred, which also promoted a sharpening of the edges in the charred structures. The features in the SEM images did not indicate a severe difference in the deposition of secondary char between sample U2 and W1. Overall, the analysis of the features in the SEM images (in Fig. 4) indicate a consistent increase in porosity in the pyrochar when prepared at temperatures from 500 °C, which was in a good agreement with the trend observed in the gas adsorption analyses. The mineral matter content in non-leached beech wood was not substantial (Table 1), so the effect of its removal was not visible in the SEM images. Differences in the morphology caused by leaching could be observed for samples pyrolysed at a temperature of 300 °C, where the leached samples presented less surface roughness in comparison to non-leached samples. However, with an increase in pyrolysis temperature, differences in morphology faded out, and the corresponding samples presented very similar in SEM images.

The non-leached particle with length 16 mm (U2) pyrolysed at 900 °C was selected for TEM analysis due to its noticeable deviation in the development of porosity with respect to temperature of pyrolysis. The features in the TEM images of sample U2 presented in Fig. 5, indicate its highly porous structure both in the microporous and mesoporous region, and are consistent with the gas adsorption results. Similar as in the SEM images, the structures indicated the presence of secondary char. Note that any other out of ordinary structures were not observed in the TEM images of sample U2. It is suspected that the inability to observe secondary char directly in the SEM and TEM images could have been related to its uneven distribution during formation. Any visible indicators of secondary char should be located in parts of the particle where the deposition most likely occurred, so in structures located close to the end of the volatiles escape path. In the investigated case, the deposition place is expected to be located at the top and at the bottom of the cylinder. However, prior to the analytical investigation, the samples had been homogenised, so the precise selection of material from specific places in the particle was no longer possible. In consequence, a conclusive indication as to what is the cause of why sample U2 behaved differently during processing at 900 °C could not be determined.

4. Conclusions

In this study, relationships between the composition (i.e. elemental composition) and yield of bio-based pyrochars and process parameters were presented, which were relatively straightforward and easy to control. Finding reliable relations between the process parameters and structural characteristics of bio-based pyrochars required, although additional efforts. From the conducted assessment of measurement methods (N_2 and CO_2 adsorption) and their processing (with non-pore specific and pore specific methods), systematic errors and biases of currently used approaches were indicated – most notably in the BET method using N_2 adsorption data. Combined application of CO_2 and N_2 adsorption analysis and proper assessment of the results allowed to propose a new data processing method which provided consistent and repeatable results (5% deviation of total specific surface area (SSA), between consecutive N_2 and CO_2 adsorption measurements).

The new approach allowed to observe reliable trends between process parameters (temperature, particle length and leaching pre-treatment) and SSA of bio-based pyrochars. The SSA of micropores and mesopores rose monotonically with the temperature used for pyrolysis up to 900 °C, without the occurrence of a peak for the pyrochars prepared at 700 °C. The influence of the particle length had a substantial effect on the microporous SSA, as opposed to the effect of leaching, which had a negligible effect. In general, the increase of pyrolysis temperature from 300 °C to 900 °C caused the formation of an additional microporous SSA in the 10 mm particles by 671 ± 4 m^2/g and in the 16 mm particles by 585 ± 23 m^2/g. The mesoporous SSA for the same temperature increment increased on average by 73 ± 6 m^2/g for all

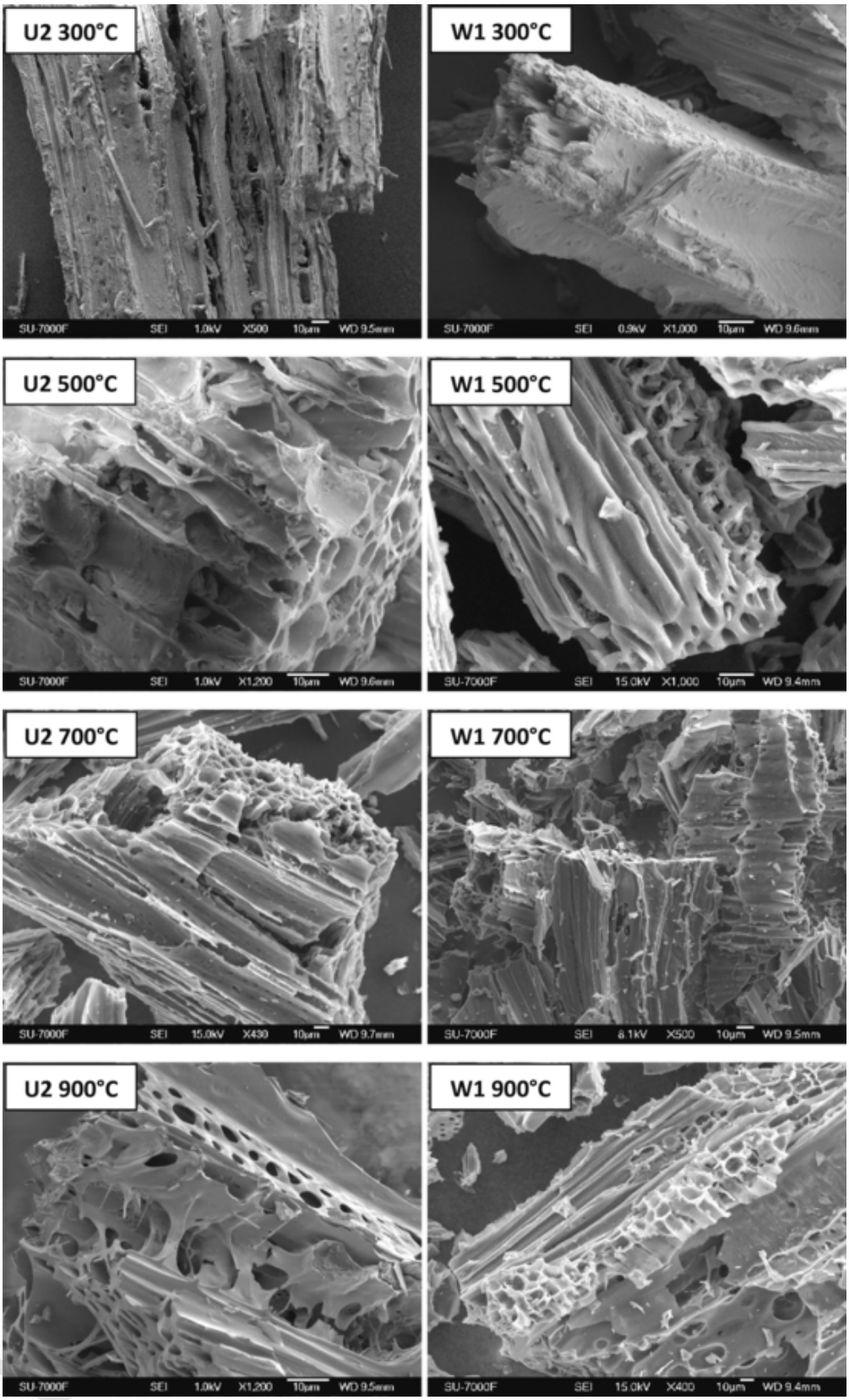

Fig. 4. SEM images of pyrolysed beech wood; left - non-leached samples with 16 mm length (U2) and right - leached with length 10 mm (W1), both produced in 300 ˚C, 500 ˚C, 700 ˚C, 900 ˚C.

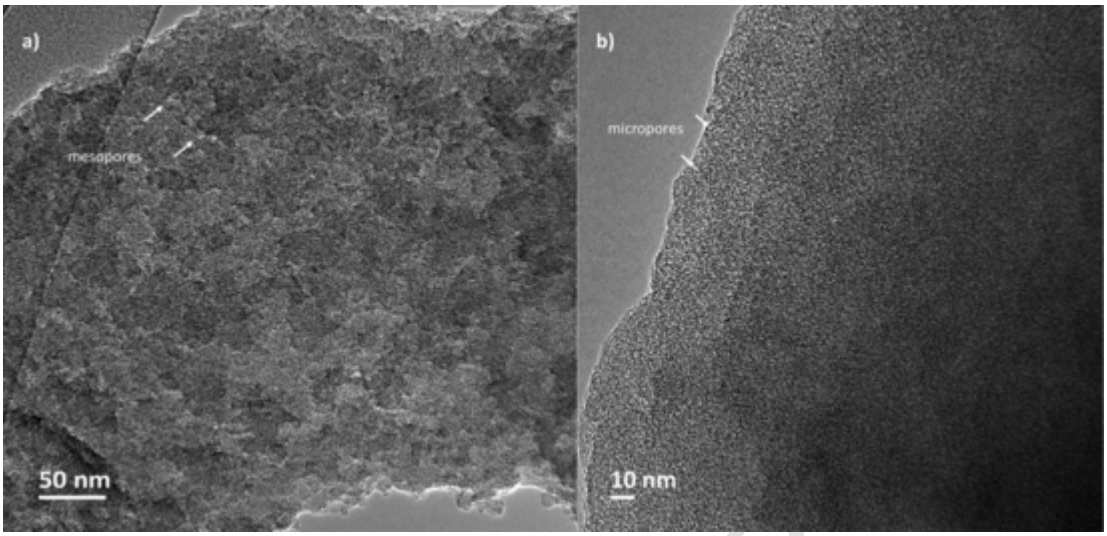

Fig.5. TEM images of the non-leached particle with length 16 mm (U2) pyrolysed at 900 °C (a – mesostructure, b – microstructure).

samples, however the trend in its development with production parameters was different than for the microporous SSA.

We expect this new approach for analysis of porosity in pyrochars should be of interest in relation to several applications and in particular useful for further development and tailoring of bio-based pyrochars as materials for electrodes in supercapacitors. For such electrodes, it seems advisable to apply the highest processing temperature (900 °C), to obtain the highest SSA and sufficient carbonisation of material (high electrical conductivity). Moreover, the used bio-based material should be acid leached and be physical short in the longitudinal direction to reduce the effect of secondary char formation within the material and prevent the undesired influence of alkali and alkaline earth metal ions during the pyrolysis. Further studies of these kinds of pyrochars as electrode materials are expected.

CRediT authorship contribution statement

Przemyslaw Maziarka: Conceptualization, Investigation, Formal analysis, Writing - original draft. **Peter Sommersacher:** Investigation, Writing - review & editing. **Xia Wang:** Investigation. **Norbert Kienzl:** Conceptualization, Supervision, Writing - review & editing. **Stefan Retschitzegger:** Project administration, Funding acquisition, Resources. **Wolter Prins:** Supervision, Writing - review & editing. **Niklas Hedin:** Supervision, Resources, Writing - review & editing. **Frederik Ronsse:** Supervision, Conceptualization, Funding acquisition, Writing - review & editing.

Declaration of Competing Interest

The authors declare that they have no known competing financial interests or personal relationships that could have appeared to influence the work reported in this paper.

Acknowledgements

Authors would like to thank Maciej Olszewski and Pablo Arauzo from Prof. Dr Andrea Kruse's research group (Universität Hohenheim) for help with the adsorption measurements and Prof. Dr Alba Diéguez-Alonso (Otto-von-Guericke-Universität Magdeburg) for help with interpretation of the adsorption results. This research was co-funded by the GreenCarbon project and Brisk2 project. The GreenCarbon project has received funding from the European Union's Horizon 2020 research and innovation programme under the Marie Skłodowska-Curie grant agreement No 721991. The Brisk2 project has received funding from the European Union's Horizon 2020 research and innovation programme under the grant agreement No 731101.

Appendix A. Supplementary material

Supplementary data to this article can be found online at https://doi.org/10.1016/j.apenergy.2020.116431.

References

[1] M. Horn, J. MacLeod, M. Liu, J. Webb, N. Motta Supercapacitors: a new source of power for electric cars? Econ Analy Policy 2019;61:93–103.
[2] S. Liu, L.i. Wei, H. Wang Review on reliability of supercapacitors in energy storage applications. Appl Energy 2020;278:115436.
[3] Z. Zhang, X. Zhang, W. Chen, Y. Rasim, W. Salman, H. Pan, et al. A high-efficiency energy regenerative shock absorber using supercapacitors for renewable energy applications in range extended electric vehicle. Appl Energy 2016;178:177–188.
[4] K. Persson, V.A. Sethuraman, L.J. Hardwick, Y. Hinuma, Y.S. Meng, A. van der Ven, et al. Lithium diffusion in graphitic carbon. J Phys Chem Lett 2010;1(8):1176–1180.
[5] F. Béguin, V. Presser, A. Balducci, E. Frackowiak Carbons and electrolytes for advanced supercapacitors. Adv Mater 2014;26(14):2219–2251.
[6] T.E. Rufford, D. Hulicova-Jurcakova, K. Khosla, Z. Zhu, G.Q. Lu Microstructure and electrochemical double-layer capacitance of carbon electrodes prepared by zinc chloride activation of sugar cane bagasse. J Power Sources 2010;195(3):912–918.
[7] A. Burke R&D considerations for the performance and application of electrochemical capacitors. Electrochim Acta 2007;53:1083–1091.
[8] F. Yao, D.T. Pham, Y.H. Lee Carbon-based materials for lithium-ion batteries, electrochemical capacitors, and their hybrid devices. ChemSusChem 2015;8(14):2284–2311.
[9] Poonam, K. Sharma, A. Arora, S.K. Tripathi Review of supercapacitors: materials and devices. J Storage Mater 2019;21:801–825.
[10] P. Kalyani, A. Anitha Biomass carbon & its prospects in electrochemical energy systems. Int J Hydrogen Energy 2013;38:4034–4045.
[11] X.-F. Tan, S.-B. Liu, Y.-G. Liu, Y.-l. Gu, G.-M. Zeng, X.-J. Hu, et al. Biochar as potential sustainable precursors for activated carbon production: multiple applications in environmental protection and energy storage. Bioresource Technol 2017;227:359–372.
[12] Y.u. Gao, L. Li, Y. Jin, Y.u. Wang, C. Yuan, Y. Wei, et al. Porous carbon made from rice husk as electrode material for electrochemical double layer capacitor. Appl Energy 2015;153:41–47.
[13] F. Barzegar, A. Bello, J.K. Dangbegnon, N. Manyala, X. Xia Asymmetric supercapacitor based on activated expanded graphite and pinecone tree activated carbon with excellent stability. Appl Energy 2017;207:417–426.
[14] W. Sun, S.M. Lipka, C. Swartz, D. Williams, F. Yang Hemp-derived activated carbons for supercapacitors. Carbon 2016;103:181–192.
[15] R.S. Gabhi, D.W. Kirk, C.Q. Jia Preliminary investigation of electrical conductivity of monolithic biochar. Carbon 2017;116:435–442.
[16] D.-J. Ryu, R.-G. Oh, Y.-D. Seo, S.-Y. Oh, K.-S. Ryu Recovery and electrochemical performance in lithium secondary batteries of biochar derived from rice straw. Environ Sci Pollut Res 2015;22(14):10405–10412.
[17] L. Zhang, J. Jiang, N. Holm, F. Chen Mini-chunk biochar supercapacitors. J Appl Electrochem 2014;44(10):1145–1151.

[18] H. Shao, Y.-C. Wu, Z. Lin, P.-L. Taberna, P. Simon Nanoporous carbon for electrochemical capacitive energy storage. Chem Soc Rev 2020;49(10):3005–3039.
[19] H. Shi Activated carbons and double layer capacitance. Electrochim Acta 1996;41(10):1633–1639.
[20] W. Gu, G. Yushin Review of nanostructured carbon materials for electrochemical capacitor applications: advantages and limitations of activated carbon, carbide-derived carbon, zeolite-templated carbon, carbon aerogels, carbon nanotubes, onion-like carbon, and graphene: Nanostructured carbon materials for electrochemical capacitor applications. WIREs Energy Environ 2014;3(5):424–473.
[21] A. Ghosh, Y.H. Lee Carbon-based electrochemical capacitors. ChemSusChem 2012;5(3):480–499.
[22] A. Noori, M.F. El-Kady, M.S. Rahmanifar, R.B. Kaner, M.F. Mousavi Towards establishing standard performance metrics for batteries, supercapacitors and beyond. Chem Soc Rev 2019;48(5):1272–1341.
[23] T.A. Centeno, O. Sereda, F. Stoeckli Capacitance in carbon pores of 0.7 to 15 nm: a regular pattern. Phys Chem Chem Phys 2011;13(27):12403.
[24] C. Largeot, C. Portet, J. Chmiola, P.-L. Taberna, Y. Gogotsi, P. Simon Relation between the ion size and pore size for an electric double-layer capacitor. J Am Chem Soc 2008;130(9):2730–2731.
[25] D. Lozano-Castelló, D. Cazorla-Amorós, A. Linares-Solano, S. Shiraishi, H. Kurihara, A. Oya Influence of pore structure and surface chemistry on electric double layer capacitance in non-aqueous electrolyte. Carbon 2003;41(9):1765–1775.
[26] S. Pohlmann, B. Lobato, T.A. Centeno, A. Balducci The influence of pore size and surface area of activated carbons on the performance of ionic liquid based supercapacitors. Phys Chem Chem Phys 2013;15(40):17287–17294.
[27] A. Kajdos, A. Kvit, F. Jones, J. Jagiello, G. Yushin Tailoring the pore alignment for rapid ion transport in microporous carbons. J Am Chem Soc 2010;132(10):3252–3253.
[28] G.G. Stavropoulos Precursor materials suitability for super activated carbons production. Fuel Process Technol 2005;86(11):1165–1173.
[29] J.S. McDonald-Wharry, M. Manley-Harris, K.L. Pickering Reviewing, combining, and updating the models for the nanostructure of non-graphitizing carbons produced from oxygen-containing precursors. Energy Fuels 2016;30(10):7811–7826.
[30] D.B. Wiedemeier, S. Abiven, W.C. Hockaday, M. Keiluweit, M. Kleber, C.A. Masiello, et al. Aromaticity and degree of aromatic condensation of char. Org Geochem 2015;78:135–143.
[31] M. Keiluweit, P.S. Nico, M.G. Johnson, M. Kleber Dynamic molecular structure of plant biomass-derived black carbon (Biochar). Environ Sci Technol 2010;44(4):1247–1253.
[32] F. Ronsse, S. van Hecke, D. Dickinson, W. Prins Production and characterization of slow pyrolysis biochar: influence of feedstock type and pyrolysis conditions. GCB Bioenergy 2013;5(2):104–115.
[33] Dieguez-Alonso A, Funke A, Anca-Couce A, Rombolà AG, Ojeda G, Bachmann J, et al. Towards biochar and hydrochar engineering—influence of process conditions on surface physical and chemical properties, thermal stability, nutrient availability, toxicity and wettability. Energies 2018;11:496.
[34] R.A. Brown, A.K. Kercher, T.H. Nguyen, D.C. Nagle, W.P. Ball Production and characterization of synthetic wood chars for use as surrogates for natural sorbents. Org Geochem 2006;37(3):321–333.
[35] C.E. Brewer, V.J. Chuang, C.A. Masiello, H. Gonnermann, X. Gao, B. Dugan, et al. New approaches to measuring biochar density and porosity. Biomass Bioenergy 2014;66:176–185.
[36] E.R. Buiel, A.E. George, J.R. Dahn Model of micropore closure in hard carbon prepared from sucrose. Carbon 1999;37(9):1399–1407.
[37] M. Thommes, K. Kaneko, V. Neimark Alexander, P. Olivier James, F. Rodriguez-Reinoso, J. Rouquerol, et al. Physisorption of gases, with special reference to the evaluation of surface area and pore size distribution (IUPAC Technical Report). Pure Appl Chem 2015;1051.
[38] Rouquerol J, Llewellyn P, Rouquerol F. Is the bet equation applicable to microporous adsorbents? In: Llewellyn PL, Rodriquez-Reinoso F, Rouqerol J, Seaton N, editors. Studies in surface science and catalysis. Elsevier; 2007. p. 49–56.
[39] H.J. Bachmann, T.D. Bucheli, A. Dieguez-Alonso, D. Fabbri, H. Knicker, H.-P. Schmidt, et al. Toward the standardization of biochar analysis: the COST action TD1107 interlaboratory comparison. J Agric Food Chem 2016;64(2):513–527.
[40] J.A. Ippolito, L. Cui, C. Kammann, N. Wrage-Mönnig, J.M. Estavillo, T. Fuertes-Mendizabal, et al. Feedstock choice, pyrolysis temperature and type influence biochar characteristics: a comprehensive meta-data analysis review. Biochar 2020;2(4):421–438.
[41] V. Gargiulo, A. Gomis-Berenguer, P. Giudicianni, C.O. Ania, R. Ragucci, M. Alfè Assessing the potential of biochars prepared by steam-assisted slow pyrolysis for CO2 adsorption and separation. Energy Fuels 2018;32(10):10218–10227.
[42] G. Sigmund, T. Hüffer, T. Hofmann, M. Kah Biochar total surface area and total pore volume determined by N2 and CO2 physisorption are strongly influenced by degassing temperature. Sci Total Environ 2017;580:770–775.
[43] F. Rouquerol Adsorption by powders and porous solids: principles, methodology and applications. Oxford: Academic press; 2014.
[44] J. Silvestre-Albero, A. Silvestre-Albero, F. Rodríguez-Reinoso, M. Thommes Physical characterization of activated carbons with narrow microporosity by nitrogen (77.4K), carbon dioxide (273K) and argon (87.3K) adsorption in combination with immersion calorimetry. Carbon 2012;50(9):3128–3133.
[45] P.I. Ravikovitch, A. Vishnyakov, R. Russo, A.V. Neimark Unified approach to pore size characterization of microporous carbonaceous materials from N2, Ar, and CO2 adsorption isotherms †. Langmuir 2000;16(5):2311–2320.
[46] A.V. Neimark, Y. Lin, P.I. Ravikovitch, M. Thommes Quenched solid density functional theory and pore size analysis of micro-mesoporous carbons. Carbon 2009;47(7):1617–1628.
[47] A.G. Liden, F. Berruti, D.S. Scott A kinetic model for the production of liquids from flash pyrolysis of biomass. Chem Eng Commun 1988;65:207–221.
[48] P.J. Arauzo, P.A. Maziarka, M.P. Olszewski, R.L. Isemin, N.S. Muratova, F. Ronsse, et al. Valorization of the poultry litter through wet torrefaction and different activation treatments. Sci Total Environ 2020;732:139288.
[49] K. Raveendran, A. Ganesh, K.C. Khilar Influence of mineral matter on biomass pyrolysis characteristics. Fuel 1995;74(12):1812–1822.
[50] P.R. Patwardhan, J.A. Satrio, R.C. Brown, B.H. Shanks Influence of inorganic salts on the primary pyrolysis products of cellulose. Bioresour Technol 2010;101(12):4646–4655.
[51] L. Rodríguez-Machín, L.E. Arteaga-Pérez, R.A. Pérez-Bermúdez, Y. Casas-Ledón, W. Prins, F. Ronsse Effect of citric acid leaching on the demineralization and thermal degradation behavior of sugarcane trash and bagasse. Biomass Bioenergy 2018;108:371–380.
[52] M. Dall'Ora, P.A. Jensen, A.D. Jensen Suspension combustion of wood: influence of pyrolysis conditions on char yield, morphology, and reactivity. Energy Fuels 2008;22(5):2955–2962.
[53] H. Almuina-Villar, N. Lang, A. Anca-Couce, J. Röpcke, F. Behrendt, A. Dieguez-Alonso Application of laser-based diagnostics for characterization of the influence of inorganics on the slow pyrolysis of woody biomass. J Anal Appl Pyrol 2019;140:125–136.
[54] T. Dahou, F. Defoort, M. Jeguirim, C. Dupont Towards understanding the role of K during biomass steam gasification. Fuel 2020;282:118806.
[55] Sommersacher P, Kienzl N, Brunner T, Obernberger I. Simultaneous online determination of S, Cl, K, Na, Zn, and Pb release from a single particle during biomass combustion. Part 1: Experimental setup–implementation and evaluation. Energy Fuels 2015;29:6734–46.
[56] Sommersacher P, Kienzl N, Brunner T, Obernberger I. Simultaneous online determination of S, Cl, K, Na, Zn, and Pb release from a single particle during biomass combustion. Part 2: Results from test runs with spruce and straw pellets. Energy Fuels 2016;30:3428–40.
[57] A. Anca-Couce, P. Sommersacher, R. Scharler Online experiments and modelling with a detailed reaction scheme of single particle biomass pyrolysis. J Anal Appl Pyrol 2017;127:411–425.
[58] S.D. Stefanidis, K.G. Kalogiannis, E.F. Iliopoulou, C.M. Michailof, P.A. Pilavachi, A.A. Lappas A study of lignocellulosic biomass pyrolysis via the pyrolysis of cellulose, hemicellulose and lignin. J Anal Appl Pyrol 2014;105:143–150.
[59] E. Ovsyannikova, P.J. Arauzo, G.C. Becker, A. Kruse Experimental and thermodynamic studies of phosphate behavior during the hydrothermal carbonization of sewage sludge. Sci Total Environ 2019;692:147–156.
[60] M.T. Reza, M.H. Uddin, J.G. Lynam, S.K. Hoekman, C.J. Coronella Hydrothermal carbonization of loblolly pine: reaction chemistry and water balance. Biomass Conv Bioref 2014;4(4):311–321.
[61] S. Lowell, J.E. Shields, M.A. Thomas Characterization of porous solids and powders surface area, pore size and density. Dordrecht: Springer; 2011.
[62] S.V. Vassilev, D. Baxter, L.K. Andersen, C.G. Vassileva, T.J. Morgan An overview of the organic and inorganic phase composition of biomass. Fuel 2012;94:1–33.
[63] K.P. Buzala, H. Kalinowska, E. Malachowska, P. Boruszewski, K. Krajewski, P. Przybysz The effect of lignin content in birch and beech Kraft cellulosic pulps on simple sugar yields from the enzymatic hydrolysis of cellulose. Energies 2019;12:11.
[64] K.T. Klasson Biochar characterization and a method for estimating biochar quality from proximate analysis results. Biomass Bioenergy 2017;96:50–58.
[65] W.J. Braida, J.J. Pignatello, Y. Lu, P.I. Ravikovitch, A.V. Neimark, B. Xing Sorption hysteresis of benzene in charcoal particles. Environ Sci Technol 2003;37(2):409–417.
[66] C. Balzer, R.T. Cimino, G.Y. Gor, A.V. Neimark, G. Reichenauer Deformation of microporous carbons during N2, Ar, and CO2 adsorption: insight from the density functional theory. Langmuir 2016;32(32):8265–8274.
[67] P. Kowalczyk, A. Ciach, A.V. Neimark Adsorption-induced deformation of microporous carbons: pore size distribution effect. Langmuir 2008;24(13):6603–6608.